© Indian Academy of Sciences

Check for updates

A new analytical protocol for high precision U–Th–Pb chemical dating of xenotime from the TTG gneisses of the Bundelkhand Craton, central India, using CAMECA SXFive Electron Probe Micro Analyzer

HIREDYA CHAUHAN[1], APARAJITA TRIPATHI[1], DINESH PANDIT[1], N V CHALAPATHI RAO[1,*] and TALAT AHMAD[2]

[1]*Mantle Petrology Laboratory, Department of Geology, Centre of Advanced Study, Institute of Science, Banaras Hindu University, Varanasi 221 005, India.*
[2]*University of Kashmir, Srinagar, India.*
Corresponding author. e-mail: nvcrao@bhu.ac.in

Xenotime is a significant accessory mineral which is being extensively used for precise U–Th–Pb geochronology by Electron Microprobe Analysis (EPMA). This paper presents a protocol for high analytical precision (<3% uncertainties on the measured ages) developed for the accurate estimation of U–Th and Pb content in xenotime using SXFive EPMA at the Department of Geology, Banaras Hindu University, by deploying five spectrometers attached with TAP, LIF, LPET, LTAP and PET crystals. The protocol is applied to the xenotime grains of tonalite-trondhjemite-granodiorite-gneiss (TTG) rocks from the geochronologically well-constrained terrain of the Bundelkhand Craton, central India. The obtained xenotime age 2929±23 Ma of TTGs is in agreement with the earlier published Neoarchaen 2697±3 Ma Pb–Pb zircon ages from the same area which validates the authenticity of the analytical method developed at the BHU-EPMA facility.

Keywords. TTG; electron microprobe; xenotime; U–Th–Pb ages; Bundelkhand Craton; India.

1. Introduction

Accessory minerals in igneous and metamorphic rocks are extremely important in understanding the crystallization evolution of the magmas and their petrologic links with major silicate assemblages besides their utility in geochronology (Hetherington *et al.* 2008; Suzuki and Kato 2008; Pandit 2018). Chemical dating of accessory minerals such as monazite, zircon, xenotime, and other Th–U–Pb bearing minerals is considered as one of the key geochronology tools for understanding the evolutionary history of magmatic and metamorphic systems. This is due to their potential to track multiple growth/deformation events in various magmatic and metamorphic conditions and also due to their ubiquitous presence in numerous rocks (Suzuki and Adachi 1991a, b; Montel *et al.* 1996; Verts *et al.* 1996; Williams *et al.* 1999; Asami *et al.* 2002, 2005; Pyle *et al.* 2005; Pant *et al.* 2009; Chew *et al.* 2011). Xenotime is one of the accessory minerals well established as a tool for geochronology, geochemistry and petrological investigations. It was first described by Swedish chemist, Jons Jacob Berzelius in 1824 from a pegmatite locality. Xenotime $[Y(HREE)PO_4]$ belongs to tetragonal

system with a zircon type structure and hosts remarkable concentration of heavy rare earth elements (HREEs) and occurs over a vast P–T regime (Hetherington *et al.* 2008; Suzuki and Kato 2008). It is an ideal mineral for U–Th–Pb geochronology because of adequate amounts of uranium–thorium concentration and is extremely resistant to diffusional Pb loss (Compston and Mathai 1994; Dahl 1997; Griffin *et al.* 2000; Fletcher *et al.* 2004; Cherniak 2006; Hetherington *et al.* 2008). Like in the case of monazite (Burger *et al.* 1965; Grauert *et al.* 1974; Köppel 1974), the concordance in U–Pb and Th–Pb ages is also observed for xenotime (Hawkins and Bowring 1997) which makes it a robust mineral for geochronology. However, xenotime is less commonly observed in many rocks due to its smaller grain size. EPMA technique has proved to be a significant tool for U–Th–Pb chemical dating (Montel 2000) and as a result, measuring the REE orthophosphate compositions of monazite and xenotime by *in-situ* methods has become increasingly common in recent years (Suzuki and Aadachi 1991a, b; Hetherington *et al.* 2008; Pandey *et al.* 2019). Recently, Hazarika *et al.* (2017) proposed an analytical protocol for U–Th–Pb dating of xenotime based on EPMA technique. They have achieved an analytical uncertainty of less than 10% in U, Th and Pb concentration.

An advanced model of EPMA, viz., SXFive of M/s CAMECA, France, was installed in April, 2016 at the Department of Geology, Institute of Science, Banaras Hindu University (BHU). The analytical conditions for silicate mineral phases as well as protocol for U–Th–Pb chemical dating of monazite using the BHU-EPMA have already been reported (Pandey *et al.* 2017, 2019). Hetherington *et al.* (2008) have suggested that EPMA methodologies applied for monazite dating are also relevant for xenotime dating because of the similar properties in the absence of reference standard. Earlier studies of xenotime chemical ages were always reported with large errors (Chatterjee *et al.* 2007; Das *et al.* 2015). Therefore, the objective of this paper is to present the analytical conditions for xenotime chemical dating based on U–Th–Pb concentration with higher accuracy and precision. For this purpose, xenotime from the TTG (tonalite-trondhjemite-granodiorite) gneiss samples (HC-25 and HC-36) from the Baghaura area (N25°10′7.2″; E78°29′5.9″) of the Bundelkhand Craton, central India, were studied and subjected to microprobe analysis (figure 1).

2. Analytical techniques and conditions for calibration and analysis

Two samples of tonalite-trondhjemite-granodiorite (TTG) gneisses, which are regarded as the basement of the Bundelkhand Craton, central India (Basu 1986; Chauhan *et al.* 2018; Pati 2020) were selected for the present research work. Well-polished thin sections were first coated by using LEICA-EM ACE 200 carbon coater to acquire thin carbon layer of 20 nm. Major and trace element analysis of xenotime were carried out by using a CAMECA SXFive EPMA equipped with five wavelength dispersive spectrometers (WDS) at the Department of Geology (Centre of Advanced Study), Institute of Science, Banaras Hindu University, Varanasi. The instrument is functional by LaB_6 electron gun source at a voltage of 15 kV, current of 40 nA and beam size of 1 μm. Five different crystals were used: thallium acid phthalate (TAP), lithium fluoride (LIF), large pentaerythritol (LPET), large thallium acid phthalate (LTAP), and pentaerythritol (PET). Internal standard-andradite has been used to verify the positions of crystals by using wavelength dispersive spectrometers (WDS). Quantification of REEs in xenotime was performed in two ways: (i) at first, the analysis of REEs was acquired at a voltage of 15 kV and 40 nA current and (ii) at second run, the analysis of other trace elements for chemical dating was acquired at a voltage of 15 kV and 200 nA current. Beam damage effects are quite obvious when high beam current density and longer beam exposure time are involved during the trace element analysis (Hetherington *et al.* 2008). For quantification and routine calibration, synthetic glass standards of all REEs have been used which were supplied by CAMECA-AMETEK. The list of the standards used in the analysis is shown in table 1.

The CAMECA SXFive Package, with SxSAB version 6.1, Cameca's PC automation (Peak-Sight[TM]) and SX-Results software, was used to carry out routine calibration, overlap correction, data acquisition, quantification, age calculations and data processing. PAP (Pouchou and Pichoir 1985) was used for matrix correction. REE analysis (La to Lu) in xenotime was carried out on LIF crystal and yttrium (Y) on LTAP, whereas Pb, Th and U were analysed on spectrometers LPET crystal and PET crystal. Selection of background values are of prime importance for trace element analysis in xenotime and background intensity for
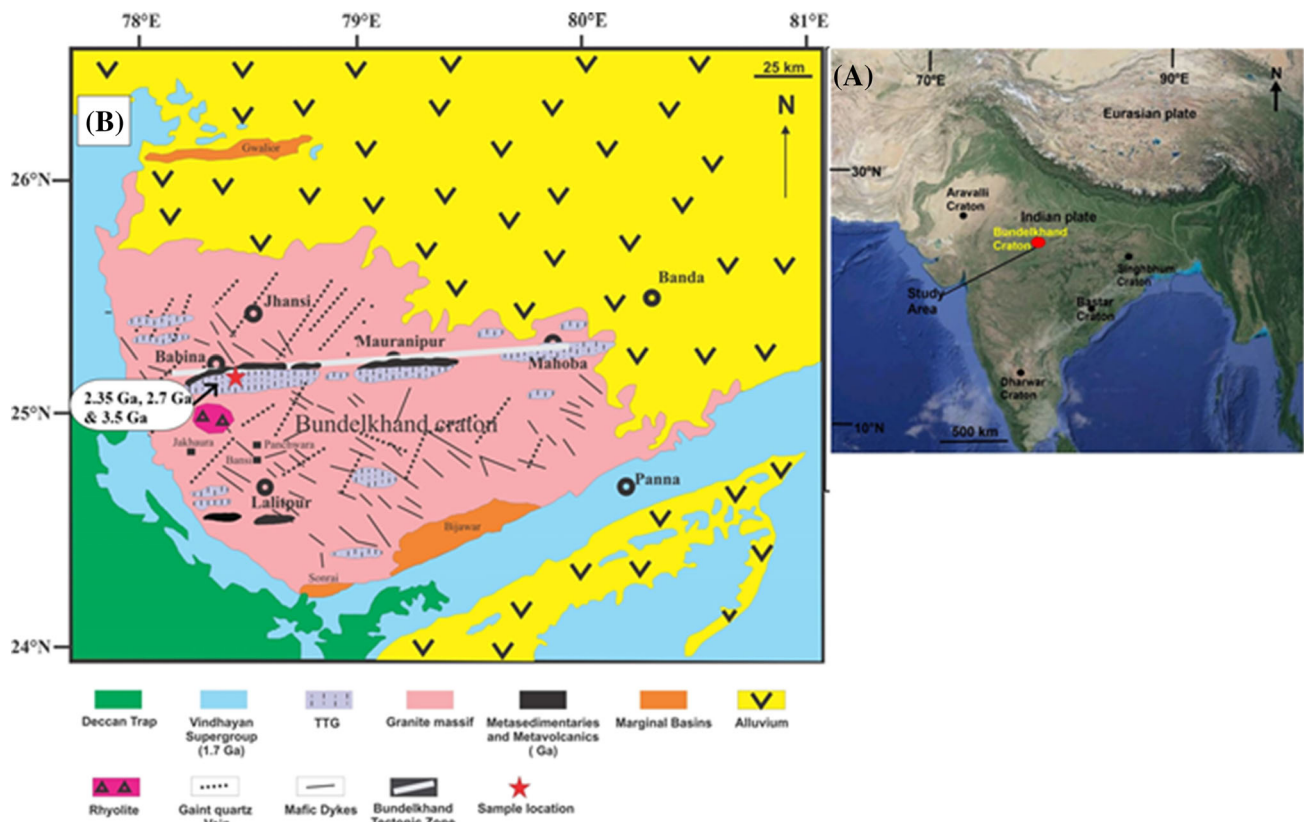
Figure 1. (**A**) Map showing the major cratons of India. (**B**) Geological map of the Bundelkhand Craton (after Basu 1986). Sample locations of the present study are marked. Ages reported by various authors are shown on the map (Sarkar *et al.* 1996; Mondal *et al.* 2002; Kaur *et al.* 2016).

Pb, Th and U. In this protocol, background values are defined in the same way as it was mentioned in monazite dating protocol reported earlier by us (Pandey *et al.* 2019). The background measurements of peak positions for Pb, Th and U were calculated from a non-linear regression of high precision wavelength dispersive scans (Williams *et al.* 2006; Jercinovic *et al.* 2008) and for other elements background values are based on linear interpolation of intensities between paired off-peak wavelength positions. For the evaluation of these analytical conditions, xenotime dating has been carried out from 20th September 2019 to 26th September 2019 (7 days), covering a time span of 153 hrs and 18 min without any interruption. X-ray spectral lines for all elements which are used in the analysis are also provided in table 1.

In this protocol, calibration for Th, U and Pb was carried out simultaneously in two different spectrometers LPET and PET. For Th analysis, M_α X-ray line was chosen and Th glass was used as a standard for the calibration of Th M_α. Background offset ranges from -1000 to $+1000$ at 200

nA. Counting time for Th calibration analysis was set to 600 s each for the background and the peak counting time fixed at 1200 s. In the U analysis, M_β line was selected and calibration for UM_β was carried out using U-glass standard at 200 nA current in spectrometers LPET and PET. Background was set between -1000 and $+1000$ for 600 s and peak counting time was also fixed at 1200 s. For Pb analysis, M_β line was preferred to avoid interference of PbM_α with YL_α lines. The calibration for PbM_β was carried out using a crocoite standard at 200 nA current through linear mode method of background estimation for 600 s and peak counting time fixed at 1200 s. The detection limits measured during this study are 70, 47, and 69 ppm for Pb, Th and U, respectively. Hetherington *et al.* (2008) mentioned that any slight change in the background measurement wavelength can affect the accuracy of the calculated age (table 2) and WDS step scans recorded in our CAMECA-SXFive instrument were used to obtain the background offsets for X-rays of UM_β, ThM_α and PbM_β lines. Hence, we have selected the background from

Table 1. *Detailed calibration setting for xenotime chemical dating by using BHU-EPMA (CAMECA SXFive). This includes X-ray spectral lines, crystal, background position, natural and synthetic standards used during the analysis.*

Element	Line	Crystal	Calibration standard	Peak time (s)	Low Bkg	High Bkg	Bkg mode	PHA mode
Si	K_α	LTAP	Wollastonite	30	−500	500	Linear	Integral
Al	K_α	LTAP	Kyanite	30	−500	500	Linear	Integral
Ca	K_α	PET	$CaSiO_3$	30	−500	500	Linear	Integral
P	K_α	PET	Apatite	30	−500	500	Linear	Integral
Y	L_α	LTAP	YAG	30	−500	500	Linear	Integral
La	L_α	LIF	La-glass	30	−500	500	Linear	Integral
Ce	L_α	LIF	Ce-glass	30	−600	400	Linear	Integral
Pr	L_β	LIF	Pr-glass	30	−500	500	Linear	Integral
Nd	L_α	LIF	Nd-glass	30	−500	500	Linear	Integral
Sm	L_β	LIF	Sm-glass	30	−500	500	Linear	Integral
Eu	L_α	LIF	Eu-glass	30	−500	500	Linear	Integral
Gd	L_β	LIF	Gd-glass	30	−500	500	Linear	Integral
Tb	L_α	LIF	Tb-glass	30	−500	500	Linear	Integral
Dy	L_α	LIF	Dy glass	30	−500	500	Linear	Integral
Ho	L_α	LIF	Ho glass	30	−500	500	Linear	Integral
Er	L_α	LIF	Er glass	30	−500	500	Linear	Integral
Tm	L_α	LIF	Tm glass	30	−500	500	Linear	Integral
Yb	L_α	LIF	Yb glass	30	−500	500	Linear	Integral
Lu	L_α	LIF	Lu glass	30	−500	500	Linear	Integral
Pb	M_β	LPET, PET	Crocoite	1200	−1000	1400	Linear	Integral
Th	M_α	LPET, PET	Th-glass	1200	−1000	1000	Linear	Integral
U	M_β	LPET, PET	U-glass	1200	−1000	1000	Linear	Integral

−1000 to +1400 as discussed by Hetherington *et al.* (2008), whereas Hazarika *et al.* (2017) have selected the background of +1350 as it was observed to be free from any interference. Similarly, all the rare earth elements (REEs) were calibrated on LIF crystal. The light rare earth elements (LREEs), based on the interference characteristics, were analysed on their specific spectral line (table 1). The calibration for the REEs was carried out with a background and peak count time of 30 s at 40 nA. For the calibration of La–L_α, an La-glass standard was used with a background value of −500 to +500. For the Ce–L_α calibration, the Ce-glass was used as a standard with the background range of −600 to +400 by avoiding any interference. In xenotime, the concentration of yttrium (Y) is much higher as compared to monazite, and an extensive care is, therefore, required while selecting the appropriate background without any interference. For Y, a YAG standard with L_α by LTAP with the background range of −500 to +500 at a peak count time of 30 s were measured. The background values for Pr–L_β, Nd–L_α, Sm–L_β, Eu–L_α, Gd–L_β, Tb–L_α, Dy–L_α, Ho–L_α, Er–L_α, Tm–L_α, Yb–L_α and Lu–$L_{\alpha-}$ all range from −500 to +500.

3. Results

TTGs from the Baghaura area consist of quartz, plagioclase, biotite, K-feldspar and hornblende. Accessory phases include zircon, chlorite, xenotime, sphene and monazite. BSE images clearly show the occurrence of variable subhedral to anhedral grains of xenotime of different sizes (figure 2A–D). Mostly, the xenotime is found to be associated within the quartz groundmass and at the contact with biotite and feldspars (figure 2). No compositional zoning is observed in any of the xenotime grains. A total of 20 chemical ages from 20 xenotime grains of two samples (HC-25 and HC-36) and one line profile of 46 out of 50 points in one single large grain of xenotime in the sample number HC-36 were recorded. The contents of U–Th–Pb in various xenotime grains of both the samples are provided in table 2 and the age profile data is shown in table 3. The probability density plot and weighted average age distribution was acquired by using the ISOPLOT program (Ludwig 2011, version 4.2) and shown in figure 3. Both the samples yielded an age population at 2929±23 Ma with 95% confidence level. A continuous line scan

Table 2. *Major and trace elements analysis and U–Pb–Th ages of xenotime grains.*

Sample number	HC-36	HC-36	HC-36	HC-25	HC-36	HC-25	HC-36	HC-36	HC-36	HC-25
Analysis point no.	10	11	12	1	13	2	14	15	16	3
SiO_2	0.13	0.73	0.86	0.18	0.23	0.12	0.59	0.41	0.58	0.13
P_2O_5	33.68	32.88	32.47	33.79	33.25	33.86	33.07	32.96	33.15	33.76
CaO	0.11	0.05	0.11	0.17	0.08	0.10	0.28	0.25	0.69	0.10
Y_2O_3	41.41	42.62	42.79	41.71	40.78	41.79	41.80	42.00	43.25	41.54
La_2O_3	0.04	0.06	0.08	0.05	0.08	0.03	0.32	0.17	0.07	0.09
Ce_2O_3	bdl	bdl	0.23	0.01	0.03	0.02	0.69	0.03	0.13	0.03
Pr_2O_3	0.01	bdl	bdl	0.00	bdl	0.09	bdl	bdl	bdl	bdl
Nd_2O_3	0.46	0.22	0.30	0.44	0.35	0.45	0.87	0.64	0.31	0.34
Sm_2O_3	0.20	0.14	0.10	0.06	0.11	0.20	0.50	0.48	0.21	0.32
Eu_2O_3	0.09	0.05	bdl	0.07	0.05	0.06	0.06	0.08	0.00	0.14
Gd_2O_3	4.02	3.54	3.48	3.80	3.48	4.11	4.09	4.46	4.05	4.12
PbO	0.35	0.55	0.49	0.51	0.21	0.35	0.24	0.27	0.17	0.34
ThO_2	0.11	1.06	1.06	0.14	0.32	0.12	0.29	0.48	0.30	0.11
UO_2	0.49	0.70	0.75	0.78	0.31	0.53	0.78	0.42	0.15	0.55
Tb_2O_3	0.52	0.44	0.45	0.43	0.52	0.54	0.51	0.63	0.55	0.54
Dy_2O_3	4.97	4.58	4.45	4.88	4.70	5.01	5.36	5.56	4.94	5.00
Ho_2O_3	2.53	2.43	2.32	2.48	2.18	2.46	2.50	2.77	2.58	2.63
Er_2O_3	4.69	4.54	4.24	4.98	4.26	4.69	4.11	3.75	3.95	4.52
Tm_2O_3	0.12	0.03	0.01	0.23	0.10	0.12	0.03	0.01	bdl	0.21
Yb_2O_3	4.41	4.23	4.42	4.41	3.88	4.33	3.63	2.69	3.11	4.43
Lu_2O_3	0.76	0.75	0.73	0.98	0.83	1.01	0.74	0.61	0.54	0.76
Total	99.08	99.60	99.33	100.09	95.74	99.99	100.45	98.66	98.75	99.67
UO_2/ThO_2	4.31	0.66	0.71	5.38	0.96	4.48	2.64	0.88	0.49	4.85
Pb (wt.%)	0.33	0.34	0.35	0.38	0.24	0.31	0.34	0.35	0.29	0.33
Th (wt.%)	0.10	0.11	0.11	0.11	0.27	0.08	0.11	0.11	0.08	0.10
U (wt.%)	0.55	0.56	0.57	0.61	0.35	0.50	0.54	0.57	0.47	0.53
Age (Ma)	2853	2854	2872	2885	2891	2893	2896	2909	2919	2934
Age error (Ma)	76	74	73	69	92	75	70	73	77	77
Age error (%)	2.7	2.6	2.5	2.4	3.2	2.6	2.4	2.5	2.6	2.6

Sample number	HC-36	HC-25	HC-36	HC-36	HC-25	HC-25	HC-25	HC-36	HC-25	HC-25
Analysis point no.	17	4	18	19	5	6	7	20	8	9
SiO_2	0.27	0.39	0.83	0.30	0.13	0.27	0.18	0.44	0.45	0.18
P_2O_5	33.97	33.55	31.55	33.82	31.74	32.74	31.84	32.99	33.06	33.78
CaO	0.13	0.04	0.30	0.11	0.15	0.03	0.05	0.06	0.06	0.57
Y_2O_3	42.44	40.81	39.94	42.40	40.72	40.31	41.63	40.12	40.09	41.23
La_2O_3	0.12	0.09	0.07	0.10	0.10	0.04	0.04	0.09	0.08	0.01
Ce_2O_3	0.01	0.02	0.12	0.06	0.07	0.12	0.01	0.13	0.15	0.13
Pr_2O_3	bdl	bdl	bdl	bdl	0.00	bdl	0.03	bdl	bdl	0.05
Nd_2O_3	0.56	0.27	0.49	0.41	0.48	0.35	0.44	0.56	0.61	0.31
Sm_2O_3	0.26	0.20	0.19	0.30	0.21	bdl	0.29	0.43	0.54	0.02
Eu_2O_3	0.06	0.01	0.01	0.03	0.03	0.01	bdl	0.02	bdl	0.25
Gd_2O_3	3.80	3.79	3.80	4.00	3.56	3.61	3.36	3.89	4.05	3.52
PbO	0.23	0.27	0.45	0.14	0.31	0.23	0.08	0.39	0.40	0.26
ThO_2	0.33	0.38	0.83	0.21	0.15	0.22	0.30	0.20	0.20	0.10
UO_2	0.25	0.49	0.89	0.31	0.46	0.31	0.01	0.93	0.94	0.41
Tb_2O_3	0.37	0.52	0.63	0.52	0.50	0.52	0.43	0.53	0.50	0.52
Dy_2O_3	4.46	4.83	5.26	5.36	4.81	4.83	4.80	5.11	4.87	4.73
Ho_2O_3	2.19	2.59	2.65	2.55	2.41	2.47	2.48	2.45	2.50	2.47
Er_2O_3	4.81	4.36	4.30	4.39	4.27	4.50	4.18	4.18	4.10	4.18
Tm_2O_3	0.15	bdl	bdl	bdl	0.10	0.05	0.12	0.06	0.18	0.14
Yb_2O_3	4.29	4.06	3.88	3.73	4.12	4.80	4.03	4.17	4.15	4.25

Table 2. *(Continued.)*

| Sample number	HC-36	HC-25	HC-36	HC-36	HC-25	HC-25	HC-25	HC-36	HC-25	HC-25
Analysis point no.	17	4	18	19	5	6	7	20	8	9
Lu_2O_3	0.98	0.69	0.81	0.92	0.94	0.97	0.83	0.86	0.97	0.66
Total	99.68	97.34	96.99	99.66	95.26	96.37	95.13	97.64	97.92	97.77
UO_2/ThO_2	0.77	1.28	1.07	1.47	3.02	1.41	0.03	4.60	4.63	4.07
Pb (wt.%)	0.32	0.20	0.39	0.28	0.18	0.19	0.18	0.33	0.17	0.18
Th (wt.%)	0.08	0.15	0.10	0.07	0.04	0.41	0.04	0.18	0.11	0.07
U (wt.%)	0.51	0.29	0.62	0.43	0.26	0.31	0.25	0.77	0.42	0.27
Age (Ma)	2949	2953	2961	2964	2966	2985	2981	2994	2994	3002
Age error (Ma)	73	120	63	78	134	112	65	82	74	93
Age error (%)	2.5	4.1	2.1	2.6	4.5	3.8	2.2	2.7	2.5	3.1
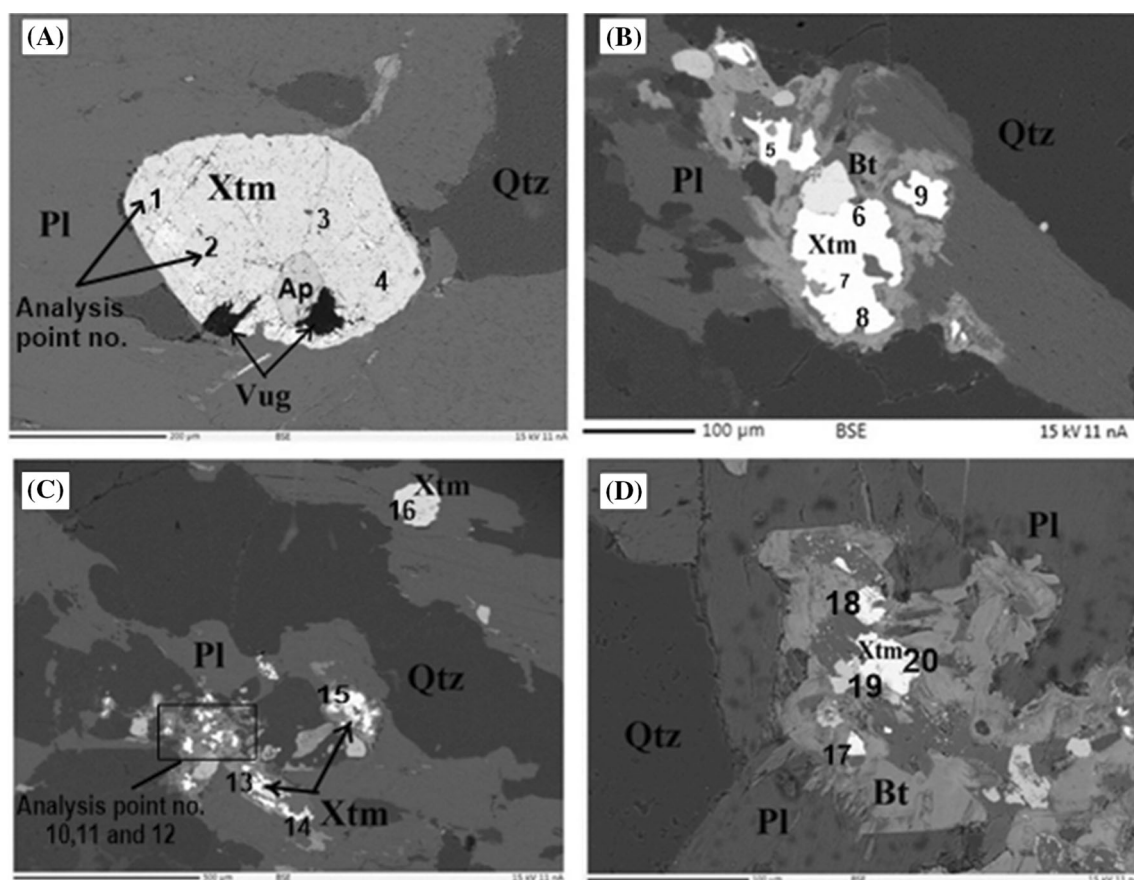
Figure 2. Backscattered electron images (BSE) of xenotime grains of variable shape and size. (**A**) Euhedral big grain of xenotime observed in the groundmass of plagioclase in sample HC-25. (**B**) Xenotime occurring as inclusion within biotite and is surrounded by the plagioclase in sample HC-25. (**C–D**) Xenotime present as inclusion in plagioclase and biotite in sample HC-36. Abbreviations are Xtm: Xenotime, Qtz: Quartz, Pl: Plagioclase, Bt: Biotite, Ap: Apatite, and vug: cavity in a mineral. Analysis spot numbers are shown on the BSE images of xenotime grains (**A–D**) as displayed in table 2.

(figure 4B) of 46 points also provided an age of 2900 Ma. Interestingly, the consistent line age data of 46 points in one single xenotime grain have recorded very low uncertainties, i.e., <3%. The chemical ages in xenotime with such very low uncertainties and high precision earlier were achieved only by Hetherington *et al.* (2008) with the help of very large pentaerythritol (VLPET) crystal installed in the CAMECASX-Ultrachron at University of Massachusetts, USA. However,

Table 3. *Line profile data of U–Th–Pb ages in xenotime from TTG sample (HC-36) of this study.*

Line scan	PbO	ThO$_2$	UO$_2$	Age (Ma)	Age error (Ma)	Age error (%)	Distance (μm)
21/3	0.32	0.09	0.53	2919	77	2.6	0
21/4	0.33	0.09	0.57	2893	75	2.6	7
21/5	0.35	0.10	0.58	2949	73	2.5	14
21/6	0.35	0.10	0.58	2973	72	2.4	21
21/7	0.35	0.10	0.58	2968	72	2.4	28
21/8	0.35	0.10	0.57	3001	73	2.4	35
21/9	0.35	0.10	0.58	2979	72	2.4	42
21/10	0.35	0.09	0.58	2982	72	2.4	49
21/11	0.34	0.09	0.55	3003	75	2.5	57
21/12	0.34	0.08	0.55	2995	75	2.5	64
21/13	0.34	0.09	0.55	3008	75	2.5	71
21/14	0.33	0.09	0.55	2954	76	2.6	78
21/15	0.34	0.08	0.55	3011	75	2.5	85
21/16	0.33	0.08	0.54	3014	76	2.5	92
21/17	0.39	0.10	0.62	3008	68	2.3	99
21/18	0.41	0.11	0.67	2981	65	2.2	106
21/19	0.42	0.11	0.68	2998	65	2.2	113
21/20	0.43	0.12	0.70	2961	63	2.1	120
21/21	0.43	0.12	0.73	2921	62	2.1	127
21/22	0.41	0.12	0.75	2792	62	2.2	134
21/24	0.44	0.12	0.73	2946	62	2.1	148
21/25	0.42	0.12	0.76	2810	61	2.2	155
21/26	0.42	0.11	0.70	2986	64	2.1	162
21/27	0.46	0.09	0.75	3011	60	2.0	169
21/28	0.49	0.09	0.82	2976	58	1.9	177
21/29	0.52	0.10	0.90	2927	55	1.9	184
21/30	0.53	0.10	0.91	2915	55	1.9	191
21/31	0.53	0.11	0.92	2917	54	1.9	198
21/33	0.46	0.18	0.94	2550	54	2.1	212
21/34	0.49	0.16	1.00	2587	53	2.0	219
21/35	0.49	0.11	0.90	2788	56	2.0	226
21/36	0.48	0.10	0.85	2841	57	2.0	233
21/37	0.46	0.10	0.89	2725	56	2.1	240
21/38	0.42	0.09	0.75	2840	62	2.2	247
21/39	0.41	0.09	0.69	2928	65	2.2	254
21/40	0.41	0.09	0.69	2948	65	2.2	261
21/41	0.36	0.09	0.58	3011	72	2.4	268
21/42	0.34	0.09	0.55	3018	74	2.5	275
21/43	0.34	0.09	0.55	3017	75	2.5	282
21/44	0.34	0.10	0.55	3010	75	2.5	290
21/45	0.32	0.09	0.52	2988	78	2.6	297
21/46	0.30	0.08	0.49	3001	81	2.7	304
21/47	0.30	0.08	0.49	2998	81	2.7	311
21/48	0.30	0.08	0.49	2994	82	2.7	318
21/49	0.31	0.09	0.50	3015	80	2.7	325
21/50	0.31	0.09	0.49	3002	81	2.7	332

BHU-EPMA has proved to be very efficient and achieved the chemical ages in xenotime with such very low uncertainties and high precision as well. These ages compare well with the published available ages (ranging from 2.35 to 3.50 Ga) for the TTGs from the same domain (Baghaura area) of the Bundelkhand craton (table 4). As these published ages were obtained by deploying other
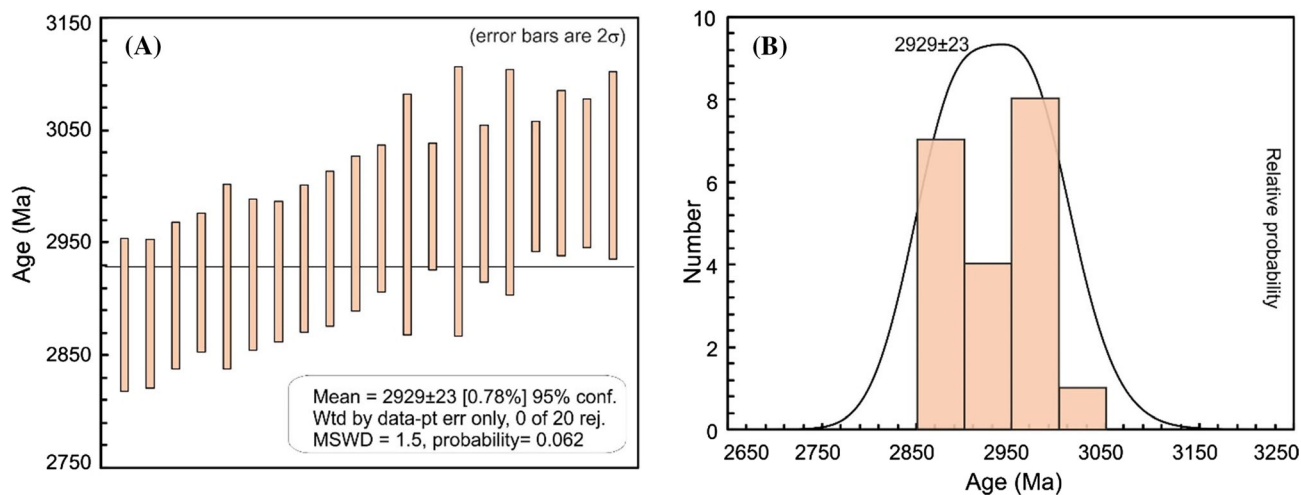
Figure 3. ISOPLOT diagram (Ludwig 2011) plotted for (**A**) weighted-average ages and (**B**) probability density ages for xenotime from TTG samples (HC-25 and HC-36) of this study with 2σ uncertainty and 20 number of point analysis.
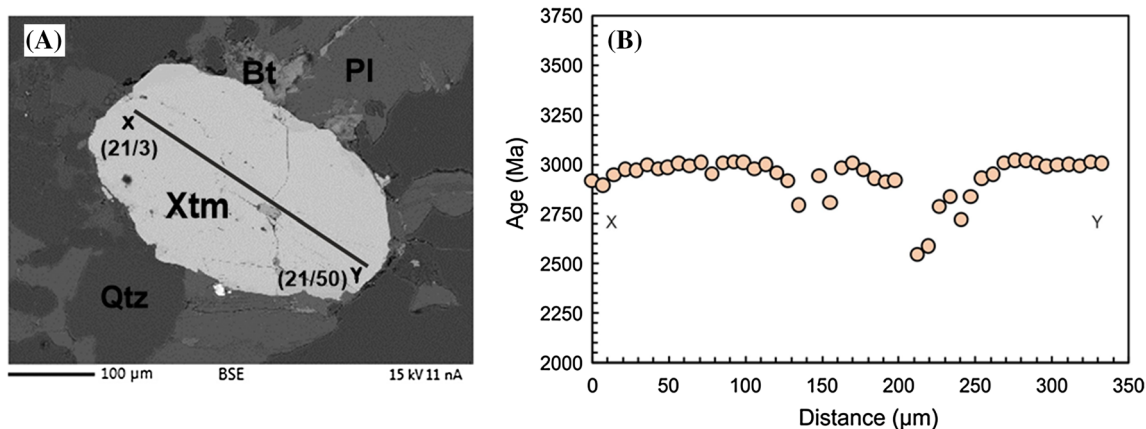

Figure 4. (**A**) BSE image of the selected single xenotime grain (sample HC-36) for the line profile analysis and (**B**) the continuous age profile graph of 46 points for single xenotime grain of this study. Abbreviations are same as mentioned in figure 2. Analysis spot numbers for X–Y line profile are shown as displayed in table 3.

Table 4. *Published Archaean TTG ages from the Baghaura area of the Bundelkhand Craton and the results from the present study.*

Age (Ma)	Mineral	Method	Reference(s)
2929±23	Xenotime	EPMA	This study
2358±46	Zircon	LA-ICP-MS	Kaur *et al.* (2016)
2697±3	Zircon	Ion Microprobe	Mondal *et al.* (2002)
3503±99	Zircon	ID-TIMS	Sarkar *et al.* (1996)

techniques and materials, viz., 3503±99 Ma (Rb–Sr whole rock isochron; Sarkar *et al.* 1996), 2697 ± 3 Ma ($^{207}Pb/^{206}Pb$ zircon ages by ion microprobe; Mondal *et al.* 2002) and 2358 ± 46 Ma (U–Pb zircon by LA-ICP-MS; Kaur *et al.* 2016), the efficacy of our methodology is supported. It should be pointed out here that the age of the TTG

suite from the Bundelkhand Craton display a wide range from 3.59 to 2.6 Ga (see Verma *et al.* 2016 and references therein). However, most reported ages are in the range of 3.5–3.0 Ga (Sarkar *et al.* 1984; Mondal *et al.* 2002; Kaur *et al.* 2014, 2016; Saha *et al.* 2016; Joshi *et al.* 2017). Therefore, our obtained xenotime age of 2.9 Ga from this domain

is within the range of earlier reported age from the geochronologically well constrained TTGs from the Bundelkhand craton.

4. Conclusions

This study presents highly improvised analytical protocol that has achieved very low uncertainties (<3%), than reported before, in the U–Th–Pb dating of xenotime using EPMA instrument at BHU and demonstrates its reliability and efficiency of the BHU-EPMA for the U–Th–Pb chemical dating of xenotime.

Author statement

Xenotime bearing samples were provided by TA. HC and AT were involved in sample preparation and EPMA data acquisition. Interpretation of chemical ages of the xenotime was carried out by HC and TA. DP contributed towards conceptual development of high precision analytical protocol, coordinated instrument operation, data acquisition and interpretation of chemical dating. NVCR provided overall supervision of the experiment. All the authors contributed in the writing up of the manuscript.

References

Asami M, Suzuki K and Grew E S 2002 Chemical Th–U–total Pb dating by electron microprobe analysis of monazite, xenotime and zircon from the Archean Napier Complex, East Antarctica: Evidence for ultra-high-temperature metamorphism at 2400 Ma; *Precamb. Res.* **114(3–4)** 249–275.

Asami M, Suzuki K and Grew E S 2005 Monazite and zircon dating by the chemical Th–U–total Pb isochron method (CHIME) from Alasheyev Bight to the SørRondane Mountains, East Antarctica: A reconnaissance study of the Mozambique Suture in eastern Queen Maud Land; *J. Geol.* **113(1)** 59–82.

Basu A K 1986 Geology of parts of the Brundelkhand granite massif central India; *Rec. Geol. Surv. India* **117(2)** 61124.

Burger A J, Von Knorring O and Clifford T N 1965 Mineralogical and radiometric studies of monazite and sphene occurrences in the Namib Desert, south-west Africa; *Mineral. Mag.* **35(271)** 519–528.

Chatterjee N, Mazumdar A C, Bhattacharya A and Saikia R R 2007 Mesoproterozoic granulites of the Shillong–Meghalaya Plateau: Evidence of westward continuation of the Prydz Bay Pan-African suture into northeastern India; *Precamb. Res.* **152(1–2)** 1–26.

Chauhan H, Saikia A and Ahmad T 2018 Episodic crustal growth in the Bundelkhand craton of central India shield: Constraints from petrogenesis of the tonalite–trondhjemite–granodiorite gneisses and K-rich granites of Bundelkhand tectonic zone; *J. Earth Syst. Sci.* **127(3)** 44, https://doi.org/10.1007/s12040-018-0945-0.

Cherniak D J 2006 Pb and rare earth element diffusion in xenotime; *Lithos* **88(1–4)** 1–14.

Chew D M, Sylvester P J and Tubrett M N 2011 U–Pb and Th–Pb dating of apatite by LA-ICPMS; *Chem. Geol.* **280** 200–216.

Compston D M and Mathai S K 1994 U–Pb age constraints on early Proterozoic gold deposits, Pine Creek Inlier, northern Australia, by hydrothermal zircon, xenotime and monazite (Abstr.); U.S. Geological Survey Circ. 1107, 65.

Dahl P S 1997 A crystal-chemical basis for Pb retention and fission-track annealing systematics in U-bearing minerals, with implications for geochronology; *Earth Planet. Sci. Lett.* **150(3–4)** 277–290.

Das S, Shukla D, Bhattacharjee S and Mitra S K 2015 Age constraints of Udayagiri domain of Nellore schist belt by xenotime dating around Pamuru, Prakasam district, Andhra Pradesh; *J. Geol. Soc. India* **85(3)** 289–298.

Fletcher I R, McNaughton N J, Aleinikoff J A, Rasmussen B and Kamo S L 2004 Improved calibration procedures and new standards for U–Pb and Th–Pb dating of Phanerozoic xenotime by ion microprobe; *Chem. Geol.* **209** 295–314.

Grauert B, Hänny R and Soptrajanova G 1974 Geochronology of a polymetamorphic and anatectic gneiss region: the Moldanubicum of the area Lam-Deggendorf, Eastern Bavaria, Germany; *Contrib. Mineral. Petrol.* **45(1)** 37–63.

Griffin B, Forbes D and McNaughton N J 2000 An evaluation of dating of diagenetic xenotime by electron microprobe; In: *An Evaluation of Dating of Diagenetic Xenotime by Electron Microprobe*, Springer, pp. 408–409.

Hawkins D P and Bowring S A 1997 U–Pb systematics of monazite and xenotime: Case studies from the Paleoproterozoic of the Grand Canyon, Arizona; *Contrib. Mineral. Petrol.* **127(1–2)** 87–103.

Hazarika P, Mishra B, Ozha M K and Pruseth K L 2017 An improved EPMA analytical protocol for U–Th–Pb total dating in xenotime: Age constraints from polygenetic Mangalwar Complex, northwestern India; *Geochemistry* **77(1)** 69–79.

Hetherington C J, Jercinovic M J, Williams M L and Mahan K 2008 Understanding geologic processes with xenotime:

Composition, chronology, and a protocol for electron probe microanalysis; *Chem. Geol.* **254** 133–147.

Jercinovic M J, Williams M L and Lane E D 2008 *In-situ* trace element analysis of monazite and other fine-grained accessory minerals by EPMA; *Chem. Geol.* **254(3–4)** 197–215.

Joshi K B, Bhattacharjee J, Rai G, Halla J, Ahmad T, Kurhila M, Heilimo E and Choudhary A K 2017 The diversification of granitoids and plate tectonic implications at the Archaean–Proterozoic boundary in the Bundelkhand Craton, central India; *Geol. Soc. London Spec. Publ.* **449(1)** 123–157.

Kaur P, Zeh A and Chaudhri N 2014 Characterisation and U–Pb–Hf isotope record of the 3.55 Ga felsic crust from the Bundelkhand Craton, northern India; *Precamb. Res.* **255** 236–244.

Kaur P, Zeh A, Chaudhri N and Eliyas N 2016 Unravelling the record of Archaean crustal evolution of the Bundelkhand Craton, northern India using U–Pb zircon–monazite ages, Lu–Hf isotope systematics, and whole-rock geochemistry of granitoids; *Precamb. Res.* **281** 384–413.

Köppel V 1974 Isotopic U–Pb ages of monazites and zircons from the crust-mantle transition and adjacent units of the Ivrea and Ceneri Zones (Southern Alps, Italy); *Contrib. Mineral. Petrol.* **43(1)** 55–70.

Ludwig K R 2011 Isoplot/Ex Version 4: A Geochronological Toolkit for Microsoft Excel: Geochronology Center; Berkeley, California, USA.

Mondal M E A, Goswami J N, Deomurari M P and Sharma K K 2002 Ion microprobe ^{207}Pb/^{206}Pb ages of zircons from the Bundelkhand massif, northern India: implications for crustal evolution of the Bundelkhand–Aravalli protocontinent; *Precamb. Res.* **117(1–2)** 85–100.

Montel J M 2000 Preservation of old U–Th–Pb ages in shielded monazite: example from the BeniBousera Hercynian kinzigites (Morocco); *J. Metamorph. Geol.* **18** 335–342.

Montel J M, Foret S, Veschambre M, Nicollet C and Provost A 1996 Electron microprobe dating of monazite; *Chem. Geol.* **131** 37–53.

Pandey M, Pandit D, Arora D, Rao N C and Pant N C 2019 Analytical Protocol for U–Th–Pb Chemical Dating of Monazite using CAMECA SXFive EPMA Installed at the Mantle Petrology Laboratory, Department of Geology, Banaras Hindu University, Varanasi, India; *J. Geol. Soc. India* **93(1)** 46–50.

Pandey R, Rao N C, Pandit D, Sahoo S and Dhote P 2017 Imprints of modal metasomatism in the post-Deccan subcontinental lithospheric mantle: Petrological evidence from an ultramafic xenolith in an Eocene lamprophyre, NW India; *Geol. Soc. London, Spec. Publ.* **463(1)** 117–136.

Pandit D 2018 Crystallization evolution of accessory minerals in Palaeoproterozoic granites of Bastar Craton, India; *Curr. Sci.* **114(11)** 2329.

Pant N C, Kundu A, Joshi S, Dey A, Bhandari A and Joshi A 2009 Chemical dating of monazite: Testing of an analytical protocol against independently dated standards; *Indian J. Geosci.* **63(3)** 311–318.

Pati J K 2020 Evolution of Bundelkhand Craton; *Episodes* **43(1)** 69–87.

Pouchou J L and Pichoir F 1985 PAP phi-rho-Z procedure for improved quantitative microanalysis. In: *Microbeam Analysis* (ed.) Armstrong J L, San Francisco Press Inc., San Francisco, pp. 104–106.

Pyle J M, Spear F S, Cheney J T and Layne G 2005 Monazite ages in the Chesham Pond Nappe, SW New Hampshire, USA: Implications for assembly of central New England thrust sheets; *Am. Mineral.* **90(4)** 592–606.

Saha L, Frei D, Gerdes A, Pati J K, Sarkar S, Patole V, Bhandari A and Nasipuri P 2016 Crustal geodynamics from the Archaean Bundelkhand Craton, India: Constraints from zircon U–Pb–Hf isotope studies; *Geol. Mag.* **153(1)** 179–192.

Sarkar A, Paul D K and Potts P J 1996 Geochronology and geochemistry of mid Archaean Trondhjemitic gneisses from Bundelkhand craton, central India; *Rec. Res. Geol.* **16** 76–92.

Sarkar A, Trivedi J R, Goplana K, Singh P N, Das A K and Paul D K 1984 Rb–Sr geochronology of the Bundelkhand granitic complex in the Jhansi–Babina–Talbehat sector, UP, India; *Indian J. Earth Sci.*, CEISM Seminar Volume, pp. 64–72.

Suzuki K and Kato T 2008 CHIME dating of monazite, xenotime, zircon and polycrase: Protocol, pitfalls and chemical criterion of possibly discordant age data; *Gondwana Res.* **14(4)** 569–586.

Suzuki K and Adachi M 1991a Precambrian provenance and Silurian metamorphism of the Tsubonasawa paragenesis in the South Kitakami terrane northwest Japan, revealed by the chemical Th–U–total Pb isochron ages of monazite, zircon and xenotime; *Geochem. J.* **25** 357–376.

Suzuki K and Adachi M 1991b The chemical Th–U–total Pb isochron ages of zircon and monazite from the gray granite of the Hida Terrane, Japan; *J. Earth Planet. Sci.* **38** 11–38.

Verma S K, Verma S P, Oliveira E P, Singh V K and Moreno J A 2016 LA-SF-ICP-MS zircon U–Pb geochronology of granitic rocks from the central Bundelkhand greenstone complex, Bundelkhand craton, India; *J. Asian Earth Sci.* **118** 125–137.

Verts L A, Chamberlain K R and Frost C D 1996 U–Pb sphene dating of metamorphism: The importance of sphene growth in the contact aureole of the Red Mountain pluton, Laramie Mountains, Wyoming; *Contrib. Mineral. Petrol.* **125** 186–199.

Williams M L, Jercinovic M J, Goncalves P and Mahan K 2006 Format and philosophy for collecting, compiling, and reporting microprobe monazite ages; *Chem. Geol.* **225(1–2)** 1–15.

Williams M L, Jercinovic M J and Terry M P 1999 Age mapping and dating of monazite on the electron microprobe: Deconvoluting multistage tectonic histories; *Geology* **27** 1023–1026.

Corresponding editor: SOMNATH DASGUPTA